(ImmPRESS™ Reagent Kit, Vector Laboratories, Burlingame, CA, USA) for 30 min. Slides were then incubated in DAB/Tris solution (three DAB/Tris tablets diluted in 150 ml distilled water; Muto Pure Chemicals, Tokyo, Japan) supplemented with 15 μl of 30% H_2O_2. Finally, the slides were counterstained with hematoxylin. Ki-67 expression was evaluated by counting 400 tumor cells in 4 high-power fields (× 200) from the micropapillary pattern areas in all 20 cases, and expressed as the percentage nuclear-stained cells.

Electron Microscopy

Three tumor specimens, already fixed with formalin and diagnosed as adenocarcinoma with the micropapillary pattern (extent: moderate and extensive), were selected and studied. Specimens were refixed in 2.5% glutaraldehyde in an isomolar phosphate buffer (pH 7.4), postfixed in 1% osmium tetroxide for 1.5 h, dehydrated in graded alcohol, and embedded in Epon 812. Ultrathin sections were mounted on copper grids, stained with uranyl acetate and lead citrate, and then examined with a JEM-1200 transmission electron microscope (Nihon Denshi, Tokyo, Japan).

Statistical Analysis

The length of disease-free survival was defined as the period from the date of surgery to the date when recurrence was diagnosed, and that of overall survival was defined as the period until the date of either death as a result of the tumor or the most recent follow-up. Survival curves were plotted using the Kaplan–Meyer method and *P*-values were calculated using the log-rank test. The correlations between several clinicopathological characteristics and histological subgroups were evaluated using the χ^2 test. *P*-values of less than 0.05 were accepted as significant. Data were analyzed with Statistical Standard Package Service Solution software (SPSS for Standard version 15.0; SPSS Inc, Chicago, IL, USA).

Results

Histological Examination

Of the 383 cases of adenocarcinoma, 103 (27%), 69 (18%), 182 (48%), and 29 (7%) were in the dominant bronchioloalveolar carcinoma, acinar, papillary, and solid with mucin subtypes, respectively (Table 1).

On histology, micropapillary tufts had no fibrovascular core and were detected in the alveolar space (Figure 1a), or in spaces inside the tumor that in most cases represented retracted connective tissue (Figure 1b), and adjacent to any of the above-mentioned four histological pattern subtypes. The micropapillary pattern was detected in 184 patients (109 men and 75 women), with 19 (11%), 33 (18%), 117 (63%), and 15 (8%) in the dominant bronchioloalveolar carcinoma, acinar, papillary, and solid with mucin subtypes, respectively (Table 1).

The extent of the micropapillary pattern present in tumors varied. The numbers of patients with focal, moderate, and extensive were 65 (35%), 85 (46%), and 34 (19%), respectively.

In the three cases studied using serial sections, we found that most tufts had continuity with other tufts and main tumor. For example, a tuft marked by (➡) in section 12 was consecutive with another tuft in section 8 and with the main tumor in section 1. Two isolated tufts, identified by (➔) in section 4, were shown to be consecutive in section 10. There also existed several tufts lacking continuity with any other tuft. The tuft marked by (→) in sections 5, 6, and 7 could not be confirmed to be continuous with any other tuft (Figure 2). Micropapillary tufts were observed to present an intricate morphology.

Immunohistochemical Findings

E-cadherin was positive at intercellular cell membranes in every micropapillary tuft, and showed no difference in staining intensity when compared with neoplastic cells in the main tumor (Figure 3a). β-Catenin staining showed the same pattern as E-cadherin (Figure 3b). Tight adhesion of cells constituting micropapillary tufts was therefore believed to be maintained. Laminin was identified in the basement membrane of normal alveolar cells and neoplastic cells of the main tumor, but on the other hand, it was not found in any cell constituting micropapillary tufts (Figure 3c). It is most likely that cells constituting micropapillary tufts had no basement membrane and therefore showed disordered continuity with the matrix. Cells constituting micropapillary tufts appeared to pile up. CD34-positive cells were enriched in the stroma of the main tumor and in the alveolar septum, whereas no CD34-positive cells were found in any micropapillary tuft (Figure 3d). No vascularity was observed in micropapillary tufts. These findings were confirmed in all 20 cases. Differences in staining pattern and intensity between cases with and without lymph node metastasis ($N = 10$ each) were not found. To determine whether cells composing micropapillary tufts had proliferation potency, Ki-67 staining was performed. Cells constituting micropapillary tufts showed positive staining for Ki-67 (Figure 3e); positive rates ranged from 5 to 45% with a mean of 20.3%. Cells constituting micropapillary tufts were therefore believed to have proliferation potency.

Electron Microscopy

Electron microscopy showed no basement membrane or vascular structures. Microvilli were some-

Table 1 Correlations between clinicopathological characteristics and the micropapillary pattern ($N=383$)

Characteristics	*No. of cases*	*Micropapillary pattern*		P-*value*
		Negative (%)	*Positive (%)*	
Gender				
Male	214	105 (53)	109 (59)	
Female	169	94 (47)	75 (41)	0.202
Age (years)				
<60	127	60 (30)	67 (36)	
≥60	256	139 (70)	117 (64)	0.193
Smoking				
Nonsmoker	185	107 (54)	80 (44)	
Smoker	198	92 (46)	104 (56)	0.044
Maximum tumor diameter (mm)				
≤30	261	139 (70)	122 (66)	
>30	122	60 (30)	62 (34)	0.457
Lymph node metastasis				
Negative	267	164 (82)	103 (56)	
Positive	126	35 (18)	81 (44)	<0.001
Pleural invasion				
Negative	265	150 (75)	115 (63)	
Positive	118	49 (25)	69 (37)	0.006
Lymphatic invasion				
Negative	215	154 (77)	61 (33)	
Positive	168	45 (23)	123 (67)	<0.001
Venous invasion				
Negative	309	182 (92)	127 (69)	
Positive	74	17 (8)	57 (31)	<0.001
Dominant histological subtype				
Bronchioloalveolar	103	84 (42)	19 (11)	
Non-bronchioloalveolar	280	115 (58)	165 (89)	<0.001
Acinar	69	36 (18)	33 (18)	
Non-acinar	314	163 (82)	151 (82)	0.968
Papillary	182	65 (33)	117 (63)	
Non-papillary	201	134 (67)	67 (37)	<0.001
Solid with mucin	29	14 (7)	15 (8)	
Non-solid with mucin	354	185 (93)	169 (92)	0.680

times observed but their distribution was focal and random. The apical and basal sides of the cells were not clearly delineated (Figure 4a), and showed intercellular junctions in micropapillary tufts (Figure 4b). These findings were confirmed in all three cases. Some cells constituting micropapillary tufts appeared to accumulate without cell polarity.

Correlation of Micropapillary Pattern and Clinicopathological Factors

Clinicopathological characteristics of patients and their tumors were compared between micropapillary pattern-positive (with focal, moderate, and extensive extent as mentioned below) and micropapillary pattern-negative groups (Table 1). Smoking ($P=0.044$), lymph node metastasis ($P<0.001$), pleural invasion ($P=0.006$), lymphatic invasion ($P<0.001$), venous invasion ($P<0.001$), dominant non-bronchioloalveolar carcinoma subtype ($P<0.001$), and dominant papillary subtype ($P<0.001$) were significantly associated with the micropapillary pattern. Especially strong correlations between the micropapillary pattern and lymph node metastasis, lymphatic invasion, and dominant non-bronchioloalveolar carcinoma subtype were observed. There was no association with gender ($P=0.202$), age ($P=0.193$), or tumor size ($P=0.457$). In stageIA cases ($N=197$), smoking ($P=0.031$), lymphatic invasion ($P<0.001$), venous invasion ($P<0.001$), dominant non-bronchioloalveolar carcinoma subtype ($P<0.001$), and dominant papillary subtype ($P<0.001$) were significantly associated with the micropapillary pattern (Table 2).

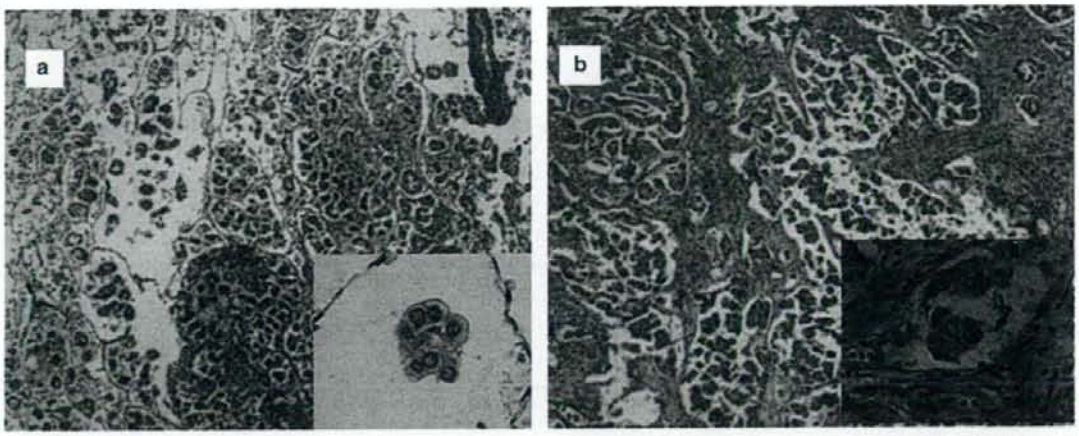

Figure 1 Representative histology of the micropapillary pattern. (**a** and **b**) The micropapillary pattern was characterized by small tufts with no fibrovascular core (**a**) lying in the alveolar space or (**b**) in spaces that in most cases represented retracted connective tissue. (**a** and **b**) Hematoxylin—eosin: ×40; inset: ×400.

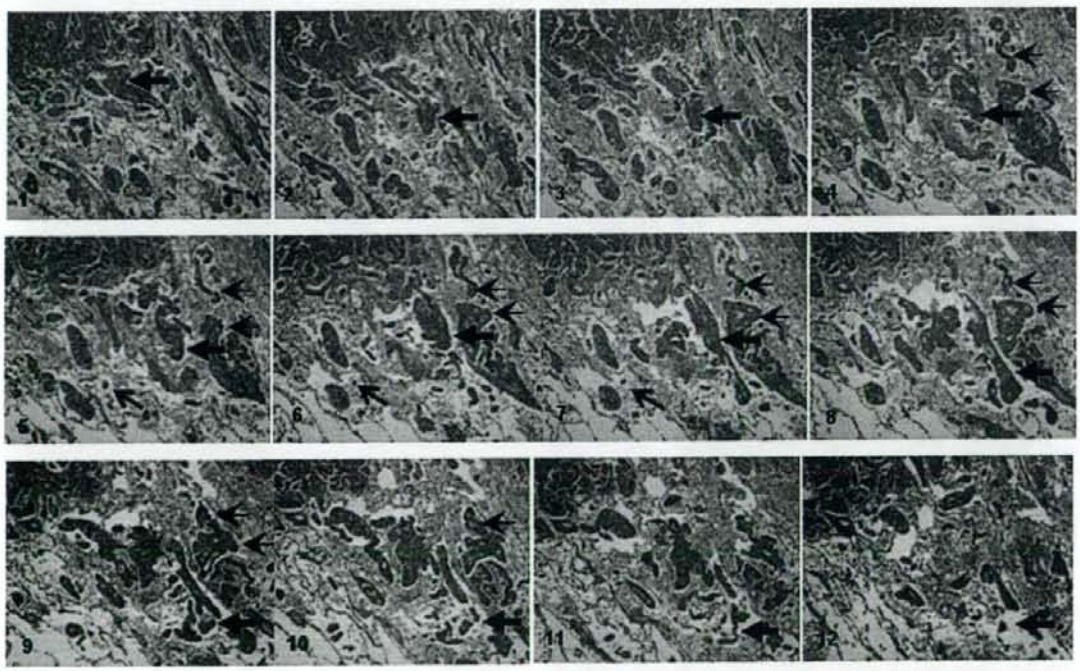

Figure 2 Serial sections of a micropapillary pattern-positive specimen. The tuft marked by (➡) in section 12 is consecutive with another tuft in section 8 and even with the main tumor in section 1. Two isolated tufts identified by (➔) in section 4 are shown to be consecutive in section 10. The tuft identified by (→) in sections 5, 6, and 7 could not be identified as continuous with any other tuft. Sections 1–16 hematoxylin–eosin at ×40.

Prognostic Significance of the Micropapillary Pattern

Survival curves showed that as the extent of the micropapillary pattern progressed, the prognosis tended to worsen, and that the disease-free and overall survival for the focal group were worse than in the none group ($P=0.027$ and $P=0.068$) (Figure 5a and b). In this study, cases in the none group (199, 52%) were therefore classified as micropapillary pattern-negative and the remainder of cases (184, 48%) were classified as micropapillary pattern-positive. Disease-free and overall survival for

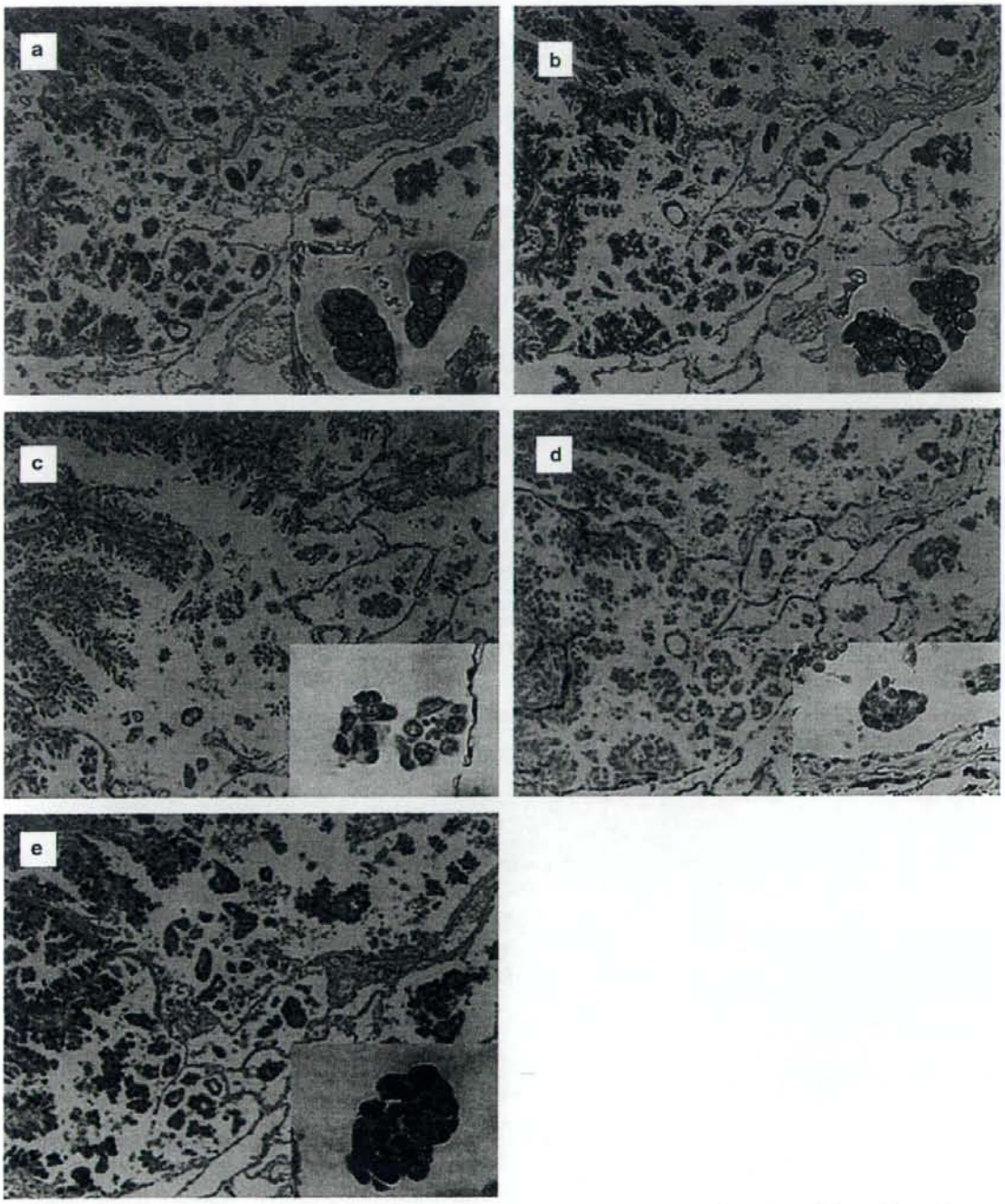

Figure 3 Immunohistochemical findings. (**a**) E-cadherin and (**b**) β-catenin were expressed at intercellular cell membranes of micropapillary tufts. (**c**) Laminin was found in the basement membrane of normal alveolar cells and in neoplastic cells in the main tumor, but was not found in cells constituting micropapillary tufts. (**d**) CD34-positive cells were enriched in the stroma of main tumor and the alveolar septum, whereas no CD34-positive cells were found in micropapillary tufts. (**e**) Cells constituting micropapillary tufts stained positive for Ki-67. (**a**) E-cadherin (**b**) β-catenin (**c**) Laminin (**d**) CD34 (**e**) Ki-67 ×40; inset: ×400.

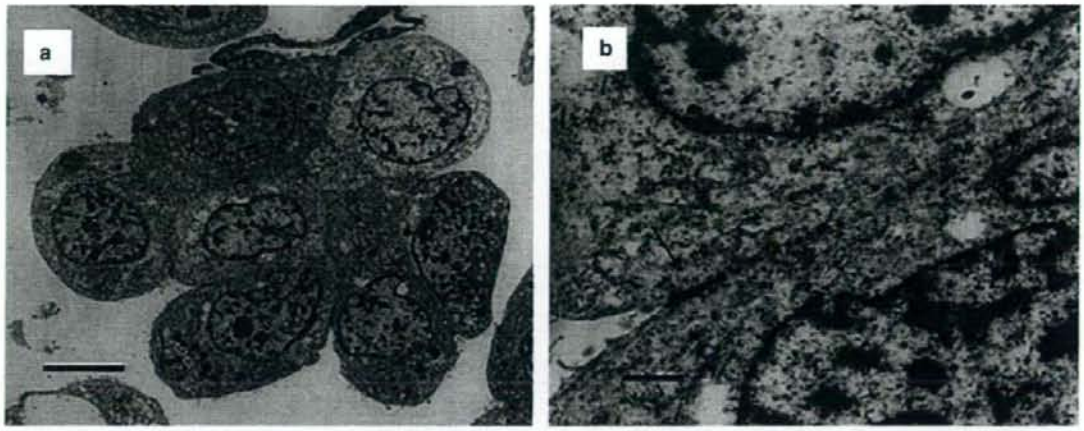

Figure 4 Electron microscopic findings. **(a)** No basement membrane or vascular structures were observed. Microvilli distribution was focal and random, and the apical and basal sides could not be clearly identified. **(b)** Intercellular junctions (arrow). **(a)** Scale bar = 5 μm; **(b)** scale bar = 500 nm.

Table 2 Correlation between clinicopathological characteristics and the micropapillary pattern in stageIA patients ($N=197$)

Characteristics	*No. of cases*	*Micropapillary pattern*		*P-value*
		Negative (%)	*Positive (%)*	
Gender				
Male	108	60 (51)	48 (62)	
Female	89	59 (49)	30 (38)	0.125
Age (years)				
<60	68	36 (30)	32 (41)	
≥60	129	83 (70)	46 (59)	0.120
Smoking				
Nonsmoker	107	72 (60)	35 (45)	
Smoker	90	47 (40)	43 (55)	0.031
Lymphatic invasion				
Negative	157	111 (93)	46 (59)	
Positive	40	8 (7)	32 (41)	<0.001
Venous invasion				
Negative	180	116 (98)	64 (82)	
Positive	17	3 (2)	14 (18)	<0.001
Dominant histological subtype				
Bronchioloalveolar	79	64 (54)	15 (19)	
Non-bronchioloalveolar	118	55 (46)	63 (81)	<0.001
Acinar	28	17 (14)	11 (14)	
Non-acinar	169	102 (86)	67 (86)	0.971
Papillary	80	34 (27)	46 (59)	
Non-papillary	117	85 (73)	32 (41)	<0.001
Solid with mucin	10	4 (3)	6 (8)	
Non-solid with mucin	187	115 (97)	72 (92)	0.176

the micropapillary pattern-positive group were significantly worse than for the micropapillary pattern-negative group ($P<0.001$ and $P=0.027$).

In all four dominant subtype groups, disease-free and overall survival rates for the micropapillary pattern-positive group tended to be worse than those for the micropapillary pattern-negative group (Figure 5c and d). The micropapillary pattern was therefore considered to affect on prognosis irrespective of dominant histological subtype.

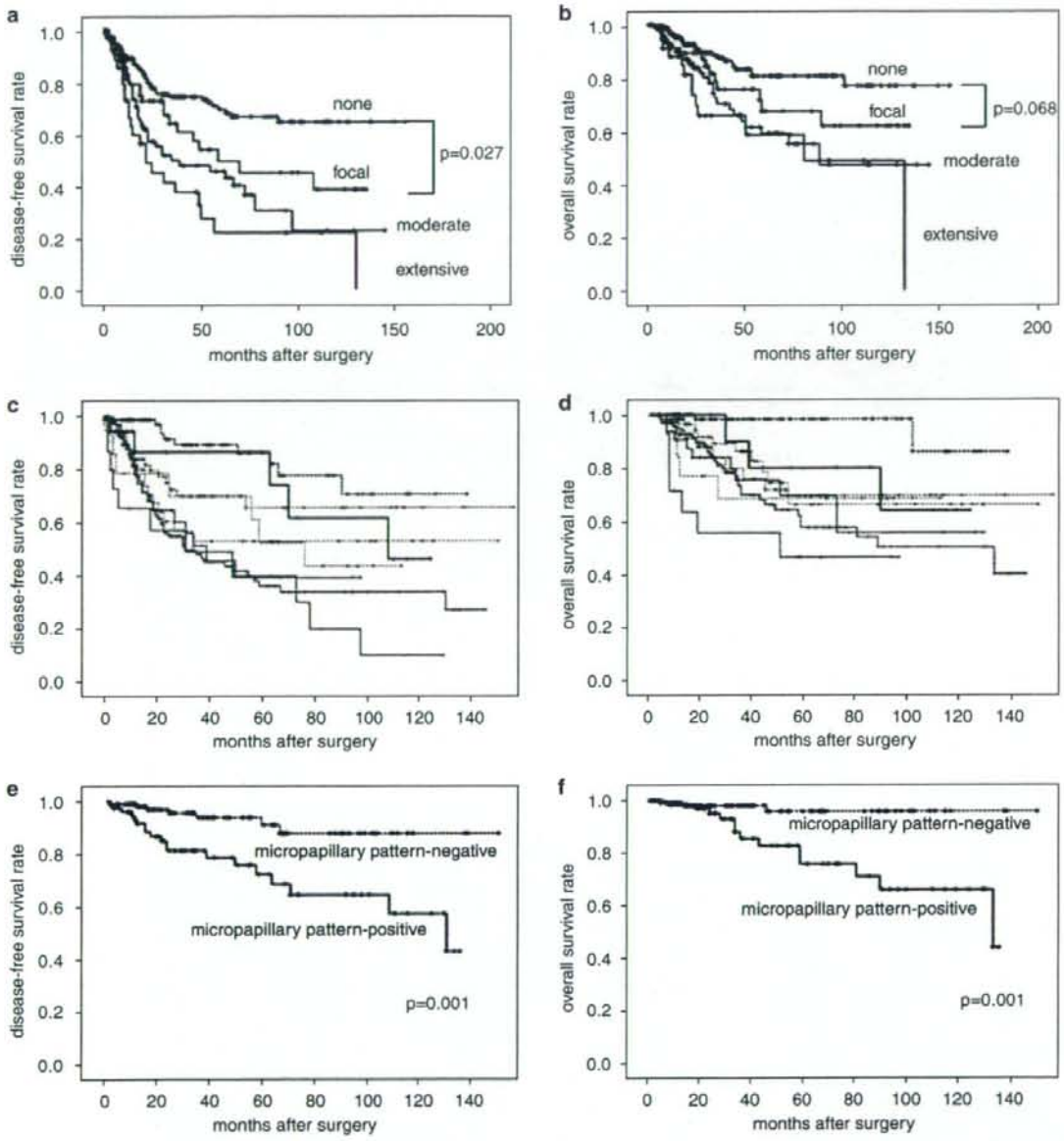

Figure 5 (**a** and **b**) Survival curves with different extents of the micropapillary pattern ($N=383$). The disease-free and overall survival of the focal group ($N=65$) were worse than those of the none group ($N=199$) ($P=0.027$ and $P=0.068$). (**c** and **d**) Survival curves grouped by the presence of the micropapillary pattern and dominant histological subtype. Black, blue, red, and green lines show dominant bronchioloalveolar carcinoma ($N=103$), acinar ($N=69$), papillary ($N=182$), and solid with mucin subtype ($N=29$), respectively. Solid and dotted lines show micropapillary pattern-positive and pattern-negative, respectively. No significant differences in survival between dominant acinar, papillary, and solid with mucin carcinomas were found. The difference between micropapillary pattern-positive and pattern-negative carcinomas was significant in the dominant papillary subtype (red) for disease-free survival ($P=0.008$) and in the dominant bronchioloalveolar carcinoma subtype (black) for overall survival ($P=0.046$). Differences were observed in other subtypes, but they were small and not significant. (**e** and **f**) The 5-year and 10-year overall survival rates of the micropapillary pattern-positive group ($N=78$) were 77.6 and 67.6%, respectively, which were significantly worse than those of the micropapillary pattern-negative group ($N=119$) (98.1 and 98.1%) in stageIA.

We then analyzed whether the micropapillary pattern had prognostic significance in the early stage when lymph node metastasis was absent at the time of surgery. At stageIA, disease-free and overall survival rates for the micropapillary pattern-positive group ($N=119$) were significantly worse than for the

micropapillary pattern-negative group ($N=78$) ($P=0.001$ and $P=0.001$) (Figure 5e and f). The 5-year and 10-year overall survival rates of the micropapillary pattern-positive group in stageIA were 77.6 and 67.6%, respectively, which were significantly worse than those of the micropapillary pattern-negative group (98.1 and 98.1%).

Discussion

On histology, micropapillary tufts were isolated from the main tumor and seemed to float in airspaces. Using serial sections, we identified an intricate structure of the micropapillary pattern in which the tufts appeared to extend into airspaces. Compared with other organs, the lung contains sufficient airspaces that cells constituting micropapillary tufts might extend easily and extensively beyond the main tumor. On histological diagnosis, it may therefore be difficult to discriminate the micropapillary pattern from intrapulmonary metastasis. However, some vascularities or stroma are normally found in intrapulmonary metastatic lesions, but not in micropapillary tufts. Both forms should be distinguished clearly. Because histopathological findings showed no vascularity in micropapillary tufts, the route of nourishment for their constitutive cells is uncertain. However, nutrients might be supplied from the surrounding epithelial lining fluids in the alveolar space.

Luna-More *et al*[13] suggested that neoplastic cells in invasive micropapillary carcinoma of the breast display reverse polarity. We explored the possibility that some of the cells constituting micropapillary tufts in lung adenocarcinomas also lost their cell polarity. Tufts composed of such cells are not micro 'papillary' but rather micro 'cluster.' Igaki *et al*[22] described that the loss of polarity in the presence of oncogenic Ras resulted in accelerated tumor invasion through the association of Ras and c-Jun N-terminal kinase pathway activation in *Drosophila*. The micropapillary pattern is believed to possess intense invasive potency considering its correlation with lymphatic, venous invasion. Loss of cell polarity might be related to this potency.

Loss of vascularity and cell–matrix contact, as well as the preservation of intercellular junctions in micropapillary tufts were demonstrated in this study. The micropapillary pattern is believed to represent the morphological piling up of neoplastic cells. Normally, when displaced from the extracellular matrix, epithelial cells undergo apoptosis (anoikis).[23] In neoplastic cells, alterations in the expression of cell–matrix adhesion molecules, integrins, integrin-associated signaling molecules, or apoptosis regulators can lead to anoikis resistance.[23–24] In the present study, we further revealed that cells constituting micropapillary tufts had proliferation potency using Ki-67 staining, and also revealed a strong correlation between the micropapillary pattern and lymphatic invasion and metastasis based on clinicopathological analysis. These cells have most likely acquired anoikis resistance and facilitated anchorage-independent growth, which are advantageous for proliferation during lymphatic cancer metastasis. The micropapillary pattern is a distinct histobiological feature that may therefore help to elucidate the mechanism of lymphatic cancer metastasis.

Our data show that survival for the focal group was worse than for the none group, and also show that as the extent of the micropapillary pattern progressed, the prognosis tended to worsen. Makimoto *et al*[21] reported no significant difference in survival between the focal (extent: $<10\%$) group and the none group, but the criteria for the extent of the micropapillary pattern and the methods used to evaluate it have been inconsistent.[20]

We clearly showed that in stageIA when lymph node metastasis was absent at the time of surgery, the 5-year and 10-year overall survival rates of the micropapillary pattern-negative group were high (98.1 and 98.1%), whereas those of the micropapillary pattern-positive group were much lower (77.6 and 67.6%). Currently, therapeutic decisions are mainly based on the TNM staging of cancer. The micropapillary pattern could be a significant prognostic factor even in the early stage.

In conclusion, the micropapillary pattern in lung adenocarcinoma is a distinct histopathological variant with biological and prognostic significance. This entity should be recognized carefully on pathological diagnosis.

Acknowledgement

This work was supported in part by a Grant-in-Aid for Scientific Research on Priority Areas 'Cancer' and for the 21st Century Center of Excellence program from the Ministry of Education, Science, Sports and Culture of Japan, for the Third Term Comprehensive 10-Year Strategy for Cancer Control from the Ministry of Health and Welfare of Japan. We thank Yuko Hashimoto, Naomichi Yagi, and Hiroshi Suzuki for technical assistance.

References

1 Alberg AJ, Samet JM. Epidemiology of lung cancer. Chest 2003;123(1 Suppl):21S–49S.
2 Jemal A, Siegal R, Ward E, *et al*. Cancer statistics. CA Cancer J Clin 2006;56:10–30.
3 Travis WD, Brambilla E, Muller-Hermelink HK, *et al*. World Health Organization Classification of Tumors: Pathology and Genetics of Tumours of Lung, Pleura, Thymus and Heart. IARC Press: Lyon, 2004, pp 26–34.
4 Noguchi M, Morikawa A, Kawasaki M, *et al*. Small adenocarcinoma of the lung. Histologic characteristics and prognosis. Cancer 1995;75:2844–2852.

5 Sobin LH, Wittenkind CH, (eds). TNM Classification of Malignant Tumours, 6th edn. Wiley-Liss: New York, 2002.
6 Beadsmoore CJ, Screaton NJ. Classification, staging and prognosis of lung cancer. Eur J Radiol 2003;45: 8–17.
7 Goya T, Asamura H, Yoshimura H, *et al*. Prognosis of 6644 resected non-small cell lung cancers in Japan: a Japanese Lung Cancer Registry Study. Lung Cancer 2005;50:227–234.
8 Kawai H, Tada A, Kawahara M, *et al*. Smoking history before surgery and prognosis in patients with stageIA non-small-cell lung cancer-a multicenter study. Lung Cancer 2005;49:63–67.
9 Sakao Y, Tomimitsu S, Takeda Y, *et al*. Carcinoembryonic antigen as a predictive factor for postoperative tumor relapse in early-stage lung adenocarcinoma. Eur J Cardiothorac Surg 2004;25:520–522.
10 Gajra A, Newman N, Gamble GP, *et al*. Impact of tumor size on survival in stageIA non-small cell lung cancer: a case for subdividing stageIA disease. Lung Cancer 2003;42:51–57.
11 Goldstein NS, Mani A, Chmielewski G, *et al*. Prognostic factors in T1 N0 M0 adenocarcinomas and bronchioloalveolar carcinomas of the lung. Am J Clin Pathol 1999;112:391–402.
12 Suzuki K, Nagai K, Yoshida J, *et al*. Predictors of lymph node and intrapulmonary metastasis in clinical stage-IA non-small cell lung carcinoma. Ann Thorac Surg 2001;72:352–356.
13 Luna-More S, Gonzalez B, Acedo C, *et al*. Invasive micropapillary carcinoma of the breast. A new special type of invasive mammary carcinoma. Pathol Res Pract 1994;190:668–674.
14 Sakamoto K, Watanabe M, De La Cruz C, *et al*. Primary invasive micropapillary carcinoma of the colon. Histopathology 2005;47:479–484.
15 Perez-Montiel D, Hes O, Michal M, *et al*. Micropapillary urothelial carcinoma of the upper urinary tract: clinicopathological study of 25 cases. Am J Clin Pathol 2006;126:86–92.
16 Bell KA, Smith Sehdev AE, Kurman RJ, *et al*. Refined diagnostic criteria for implants associated with ovarian atypical proliferative serous tumors (borderline) and micropapillary serous carcinomas. Am J Surg Pathol 2001;25:419–432.
17 Nagao T, Gaffy TA, Visscher DW, *et al*. Invasive salivary duct carcinoma. A distinct histologic variant with biologic significance. Am J Surg Pathol 2004;228:319–326.
18 Amin MB, Tamboli P, Merchant SH, *et al*. Micropapillary component in lung adenocarcinoma: a distinctive histologic feature with possible prognostic significance. Am J Surg Patho 2002;26:358–364.
19 Miyoshi T, Satoh Y, Okumura S, *et al*. Early-stage lung adenocarcinomas with a micropapillary pattern, a distinct pathologic marker for a significantly poor prognosis. Am J Surg Patho 2003;27:101–109.
20 Tsutsumida H, Nomoto M, Goto M, *et al*. A micropapillary pattern is predictive of a poor prognosis in lung adenocarcinoma, and reduced surfactant apoprotein A expression in the micropapillary pattern is an excellent indicator of a poor prognosis. Mod Pathol 2007;20:638–647.
21 Makimoto Y, Nabeshima K, Iwasaki H, *et al*. Micropapillary pattern: a distinct pathological marker to subclassify tumours with a significantly poor prognosis within small peripheral lung adenocarcinoma ($\leq$20 mm) with mixed bronchioloalveolar and invasive subtypes (Noguchi's type C tumours). Histopathology 2005;46:677–684.
22 Igaki T, Pagliarini RA, Xu T. Loss of cell polarity drives tumor growth and invasion through JNK activation in *Drosophila*. Curr Biol 2006;16:1139–1146.
23 Frisch SM, Francis H. Disruption of epithelial cell–matrix interactions induces apoptosis. J Cell Biol 1994;124:619–626.
24 Frisch SM, Ruoslahti E. Integrins and anoikis. Cur Opin Cell Biol 1997;9:701–706.

Journal of Pathology
J Pathol 2008; **216**: 75–82
Published online 13 May 2008 in Wiley InterScience
(www.interscience.wiley.com) **DOI:** 10.1002/path.2383

Original Paper

Expression profile of early lung adenocarcinoma: identification of *MRP3* as a molecular marker for early progression

S Hanada,[1,5] A Maeshima,[2,7] Y Matsuno,[2,6] T Ohta,[1] M Ohki,[1] T Yoshida,[1,3] Y Hayashi,[4] Y Yoshizawa,[5] S Hirohashi[2] and M Sakamoto[2,4]*

[1] *Center for Medical Genomics, National Cancer Center Research Institute, Tokyo, Japan*
[2] *Pathology Division, National Cancer Center Research Institute, Tokyo, Japan*
[3] *Genetic Division, National Cancer Center Research Institute, Tokyo, Japan*
[4] *Department of Pathology, Keio University School of Medicine, Tokyo, Japan*
[5] *Department of Integrated Pulmonology, Tokyo Medical and Dental University, Tokyo, Japan*
[6] *Department of Surgical Pathology, Hokkaido University Hospital, Hokkaido, Japan*
[7] *Clinical Laboratory Division, National Hospital Organization Tokyo Medical Center, Tokyo, Japan*

*Correspondence to:
M Sakamoto, Department of Pathology, Keio University School of Medicine, 35 Shinanomachi, Shinjuku-ku, Tokyo 160-0016, Japan.
E-mail: msakamot@sc.itc.keio.ac.jp

No conflicts of interest were declared.

Received: 26 February 2008
Revised: 30 April 2008
Accepted: 5 May 2008

Abstract

Early lung adenocarcinoma is well-recognized as a small-sized non-invasive adenocarcinoma or localized non-mucinous bronchioloalveolar carcinoma (LNMBAC); however, the molecular events associated with these early lesions are not clear. To determine the genes involved in tumorigenesis at the early stage of lung adenocarcinoma, we compared the mRNA expression profiles of LNMBAC and normal lungs with an oligonucleotide array. Immunohistochemical analyses were performed to confirm the expression of detected genes. We identified 183 differentially expressed genes, of which 15 were up-regulated and 168 down-regulated. Among them, most up-regulated genes, such as *AQP3* and *Claudin-4*, were expressed in both adenocarcinoma cells and type II alveolar pneumocytes, corresponding to the histological similarity between these cell types. However, multidrug resistant protein 3 (MRP3) was only expressed on tumour cell membranes and not in type II alveolar pneumocytes, as confirmed by immunohistochemistry. Moreover, the number of MRP3-positive cells significantly increased from AAH (the precursor lesion of lung adenocarcinoma) to LNMBAC. We conclude that MRP3 could be a novel molecular marker for LNMBAC, whose expression increases during the early progression of tumourigenesis.

Keywords: lung adenocarcinoma; localized non-mucinous BAC (LNMBAC); expression profile; microarray; MRP3

Introduction

Lung cancer is the leading cause of death in western countries and Japan. Among the four major histological types, adenocarcinoma is the most common, with the number of afflicted patients increasing in recent years. As lung adenocarcinomas are usually detected late in disease progression and are recalcitrant to morphological and molecular analyses, owing to their histological and cytological heterogeneity, the molecular mechanisms of adenocarcinoma tumourgenesis remain relatively unknown, especially in the early stage [1].

Introduction of high-resolution computed tomography (HRCT) to lung cancer diagnosis has made it possible to detect atypical adenomatous hyperplasia (AAH), a presumed precursor lesion or peripheral small-sized adenocarcinoma that can hardly be detected by X-ray examination [2–6]. Early lung adenocarcinoma is a novel concept and category derived from the clinicopathological analysis of small peripheral lung adenocarcinomas. Thus, this category is different from early cancer, which usually indicates stage I lung adenocarcinomas of the TMN classification. Noguchi *et al* histopathologically examined small adenocarcinomas (<2 cm) and subdivided them into two groups; those having a replacing growth structure and those having a non-replacing and destructive structure [7]. The former group includes three types: type A, a localized bronchioloalveolar carcinoma (LBAC); type B, comprised of LBAC with alveolar collapse; and type C, LBAC with active fibroblastic change. Because type A and type B adenocarcinomas, which are localized non-mucinous BAC (LNMBAC) in the World Health Organization (WHO) classification, have

no interstitial invasion, no lymph node metastasis, and their 5 year survival rates are 100%, they are categorized as early lung adenocarcinomas.

According to recent studies, the progression of lung adenocarcinoma is considered to be caused by sequential molecular events like the adenoma–carcinoma sequence of colon cancer [8]. Studying LNMBAC could be a great help in elucidating the first step of the sequential molecular events underlying tumourigenesis. Although several studies have reported molecular events involving K-ras or P53 for small adenocarcinoma or AAH, most of the molecular mechanisms of the early stage remain unclear [9–11]. Understanding the probability and interval of clinical progression from AAH to overt malignancy, as well as from early to advanced adenocarcinoma, would also be very useful for clinical management. Novel tumour markers for early adenocarcinoma may help to diagnose LNMBAC more objectively.

The microarray technique is a recently developed and powerful tool for examining the expression of a massive number of genes at one time and has proved useful in the characterization of cancers [12–14]. In the present study, to determine molecular events and to find genes that characterize early lung adenocarcinoma, we compared the gene expression of LNMBAC and normal lungs with the oligonucleotide microarray. We identified a gene set that distinguished the tumour from the normal lung and specifically found that MRP3 expression increased during the early progression of tumourigenesis, suggesting its utility as a novel molecular marker for early lung adenocarcinoma.

Materials and methods

Tissue samples

Ten lung adenocarcinomas and 10 normal lungs were obtained from patients who underwent surgical resection at National Cancer Centre Hospital, Japan, and the study was approved by the National Cancer Centre ethics review board. Of the samples, four were paired tumours and corresponding non-cancerous lung tissue from the same patients. First, small samples for molecular analysis were obtained from surgically resected specimens and immediately cut into small pieces, snap-frozen in liquid nitrogen and stored until use. The the rest of the whole resected specimens were fixed routinely in 10% formalin, cut serially into 5–7 mm slices, and macroscopically examined. From the section including the largest diameter of the tumour, all the tumour tissue as well as the surrounding lung tissue was removed and embedded in paraffin, and then cut into 4 μm sections. Haematoxylin and eosin (H&E) and elastica and Van Gieson (EVG) staining was performed. All tumours were <3 cm in diameter (range 0.7–2.7 cm) and histologically diagnosed as LNMBAC without active fibroblastic change by two individual pathologists (Figure 1 and Table 1). For immunohistochemical analysis, 15 normal lungs, 10 hyperplasias, 15 AAHs and 12 LNMBACs were analysed. Sections were prepared from formalin-fixed, paraffin-embedded tissues of surgically resected samples.

Microarray analysis

For gene expression analysis, we used the GeneChip human Genome HG-U95Av2 oligonucleotide microarray (Affymetrix, Santa Clara, CA, USA). Target cRNA for microarray hybridization was prepared as follows. Total RNA was isolated using RNeasy columns (Qiagen, Hilden, Germany) according to the manufacturer's instructions. From 5 μg total RNA, double-stranded cDNA with a T7 promoter tag was generated using the Superscript Choice system (Invitrogen), and biotin-labelled cRNA was synthesized from the double-stranded cDNA by *in vitro* transcription, using a BioArray RNA transcript-labelling kit (Enzo Diagnostics, Farmingdale, NY, USA). The cRNA was purified using RNeasy columns; 20 μg biotin-labelled cRNA was fragmented at 94 °C for 35 min in 40 μl 1× RNA fragmentation buffer (40 mM Tris/acetate, pH 8.1, 100 mM K acetate and 30 mM Mg acetate) and used for microarray hybridization. Hybridization, washing, staining, and scanning were carried out according to the manufacturer's instructions. Briefly, 10 μg biotin-labelled and fragmented cRNA was hybridized to the microarray in 200 μl 1× 4-morpholinepropanesulphonic acid (MES) hybridization buffer (100 mM MES/Na-MES, pH 6.6, 890 mM NaCl, 20 mM EDTA, 0.01% Tween 20) containing 0.1 mg/ml herring sperm DNA (Promega, Madison, WI, USA) and 0.5 mg/ml acetylated BSA (Invitrogen) at 45 °C for 16 h with rotation. Subsequently,

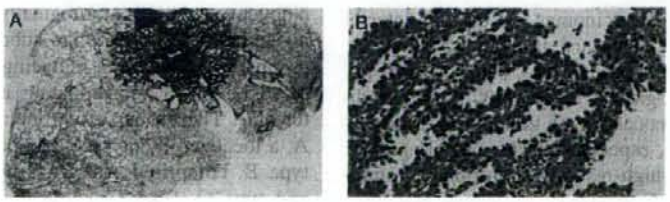

Figure 1. Histology of early lung adenocarcinoma (LNMBAC). The boundary between the tumour and the surrounding normal lung is indistinct. Each tumour cell resembles a type II pneumocyte and grows by replacing alveolar lining cells (H&E original magnification, ×400)

J Pathol 2008; **216**: 75–82 DOI: 10.1002/path

the microarrays were washed with non-stringent wash buffer (60 mM Na_2HPO_4/NaH_2PO_4, pH 7.4, 894 mM NaCl, 6 mM EDTA and 0.01% Tween 20) at 25 °C and then with stringent wash buffer (100 mM MES/Na-MES, pH 6.6 26 mM NaCl and 0.01% Tween 20) at 50 °C, stained with streptavidin–phycoerythrin (Molecular Probes) and biotinylated antistreptavidin (Vector Laboratories, Burlingame, CA, USA) and scanned with a GeneArray scanner (Hewlett-Packard, Santa Clara, CA, USA).

Data analysis

Using the Microarray Suite 4.0 software package (Affymetrix), scanned images were transformed into signals called the average difference, which represented the mean difference of signal intensities between match and mismatch probe pairs. The hybridization intensities were normalized to 1000 across all samples. Data analyses were done using Excel (Microsoft), GeneSpring (Silicon Genetics, Redwood City, CA, USA) and Cluster (Stanford) and visualized using Tree and View (Stanford).

RT–PCR

From the total RNA samples, template cDNA was synthesized with an oligo(dT) primer and Super Script Choice System (Invitrogen). PCR was performed with AmpliTaq Gold and the GeneAmp 7700 Sequence Detector (Applied Biosystems, Foster City, CA, USA). The primer sets for MRP3 were designed as 5′-CTGCTAAACCCTGACCCTCTGCGG-3′ (forward) and 5′-TCCAGCAGCTGCTGCACCACCATC-3′ (reverse). PCR conditions were as follows: 1 cycle at 94 °C for 10 min, then 30 cycles at 95 °C for 15 s, 60 °C for 1 min and 75 °C for 30 °C, followed by a final 75 °C extension for 10 min. For standardization of the amount of RNA, expression of glyceraldehyde 3-phosphate dehydrogenase (GAPDH) was quantified for each sample.

Immunohistochemistry

Immunohistochemistry was performed on formalin-fixed, paraffin-embedded tissue sections by an immunoperoxidase method, as described previously [15]. Antibodies used for immunohistochemical analysis were MRP3 (M3II-21; Signet Laboratories Inc., MA, USA) at a dilution of 1 : 100, TTF-1 (Neomarkers, Fremont, CA, USA) at a dilution of 1 : 200, AQP3 (Santa Cruz Biotechnology, Santa Cruz, CA, USA) at a dilution of 1 : 200, and Claudin-4 (Zymed Laboratories, South San Francisco, CA, USA) at a dilution of 1 : 200.

Staining evaluation

Staining was evaluated by two independent observers. The positivity index was expressed as the percentage of positive cells in each lesion.

Results

Gene expression profiling of LNMBAC

To identify genes that characterized early lung adenocarcinoma, we compared expression profiles between 10 LNMBACs and 10 normal lungs, using the oligonucleotide array. We applied two independent types of supervised analysis.

The first analysis proceeded using the following criteria. (a) Genes whose average differences (mean difference in signal intensity between perfect match and mismatch probe pairs) were >1000 in at least 5/20 samples. (b) *t*-Test with significance set at $p < 0.05$ to identify genes expressed differently between tumours and normal tissue. (c) Multiple testing corrections (Young and permutation test) applied by Gene Spring software. Multiple testing correction adjusts the individual p value for each gene to keep the overall error rate to less than or equal to the specific p value cut-off. Using these criteria, we selected 183 differentially expressed genes from 12 696 probe sets, 15 genes that were up-regulated in tumours (Table 2) and 168 down-regulated genes (Supplementary Table 1, available at: http://www.interscience.wiley.com/jpages/0022-3417/suppmat/path.2383.html). To validate that these genes could actually distinguish early adenocarcinomas from normal lungs, we applied hierarchical clustering to classify the same sample sets, using the 183 selected genes (Figure 2).

The second analysis proceeded using the following criteria. (a) Presence in tumours (i.e. exactly

Table 1. Clinicopathological feature of surgically resected specimens

Patient No.	Gender	Age	Stage	T	N	M	Histological differentiation	Vascular invasion	Lympho duct invasion	Smoking		Brinkman index
K186	F	61	IA	I	0	0	Well	–	–	+	Current	375
K187	M	55	IA	I	0	0	Well	–	–	+	Current	700
K230	F	66	IA	I	0	0	Well	–	–	–	Never	
K228	F	69	IA	I	0	0	Well	–	–	+	Current	165
K236	F	73	IA	I	0	0	Well	–	–	–	Never	
K265	M	76	IA	I	0	0	Well	–	–	+	Former	450
K269	M	52	IA	I	0	0	Well	–	–	+	Current	640
K274	M	59	IA	I	0	0	Well	–	–	+	Former	360
K303	M	65	IA	I	0	0	Well	–	–	–	Never	

Table 2. List of genes up-regulated in LNMBAC compared to normal lungs

Symbol	Affymetrix probe No.	p Value	Locus	Gene description
ABCC3	1930_at	0.016	17q22	ATP-binding cassette, sub-family C (CFTR/MRP), member 3
WFDC2	33933_at	0.001	20q12–q13.2	WAP four-disulphide core domain 2
AQP3	39248_at	0.003	9p13	Aquaporin 3
ADAM8	40712_at	0.021	10q26.3	A disintegrin and metalloproteinase domain 8
CACNB1	36557_at	0.024	17q21–q22	Calcium channel, voltage-dependent, β 1 subunit
MST1R	1317_at	0.028	3p21.3	Macrophage stimulating 1 receptor (c-met-related tyrosine kinase)
BENE	33331_at	0.032	2q13	BENE protein
CLDN4	35276_at	0.001	7q11.23	Claudin 4
KIAA0907	33885_at	0.026	1q21.2	KIAA0907 protein
KIAA0657	35780_at	0.013	2q36.3	KIAA0657 protein
GCN5L2	38628_at	0.003	17q21	GCN5 general control of amino-acid synthesis 5-like 2 (yeast)
CHC1	1196_at	0.009	1p36.1	Chromosome condensation 1
LGALS3BP	37754_at	0.003	17q25	Lectin, galactoside-binding, soluble, 3 binding protein
ITPR3	37343_at	0.032	6p21	Inositol 1,4,5-triphosphate receptor, type 3
KIAA0076	36084_at	0.032	6p21.1	KIAA0076 gene product

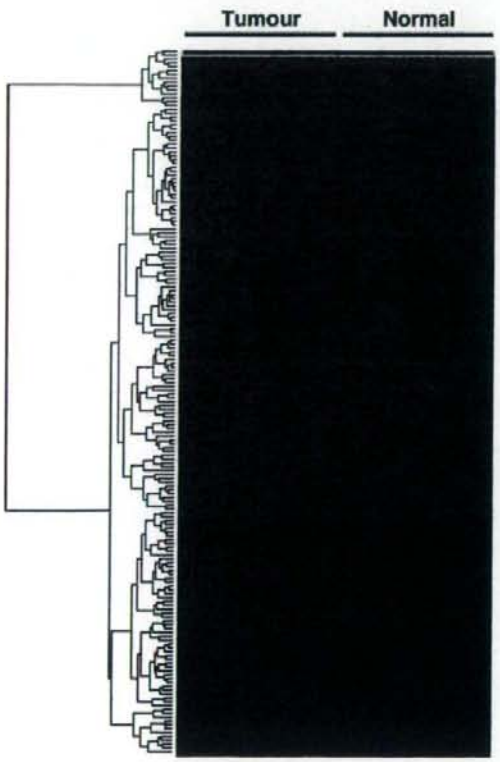

Figure 2. Expression profiling of LNMBAC. Hierarchial clustering was performed, in which 183 differentially expressed genes clearly differentiated LNMBACs from normal lungs. The normalized expression index of each transcript is indicated by a coloured bar. Up-regulated genes were expressed as red and down-regulated genes as green

expressed in the samples). (b) Average difference of >1000. (c) A > three-fold increase in average difference when compared to 10 normal sample mixtures in at least 5/10 samples. Using these criteria, we selected 140 genes that were up-regulated by more than three-fold (Supplementary Table 2, available at: http://www.interscience.wiley.com/jpages/0022-3417/suppmat/path.2383.html).

Genes expressed in both type II alveolar pneumocytes and LNMBAC

For the up-regulated genes listed in Table 2 and Supplementary Table 2, we selected interesting genes and performed immunohistochemical analysis on LNMBACs. We also examined AAH, hyperplasia and normal regions from the surrounding lung.

We examined *TTF-1*, *AQP3* and *Claudin-4* (Figure 3). We also analysed *MST1R* (*RON*), *MUC1*, *CD24*, *HNF1b*, *ARFGEF1*, *GRB7*, *AQP5* and *NQO1* (data not shown); those genes were specifically expressed in tumour cells and could not be detected in the interstitial areas in carcinoma tissue. In surrounding regions, normal type II pneumocytes were also positive in every case, whereas type I cells were negative. The staining intensity of TTF-1 in tumour cells was the same as in normal type II pneumocytes; however, that of AQP3 and Claudin-4 in tumour cells was stronger than in normal type II pneumocytes. In hyperplasia and AAH, these genes were also positive in the type II pneumocytes and atypical cells that morphologically resembled type II pneumocytes, respectively (data not shown). Therefore, these genes were considered to be related to features of type II pneumocytes.

MRP3 expression in LNMBAC

Of the genes listed in Table 2 and Supplemenatry Table 2, *MRP3* was the only one that was up-regulated more than three-fold in all 10 samples as well as being undetectable in the normal lung. (Figure 4) To confirm the mRNA level of *MRP3*, we applied RT–PCR (Figure 5). In all four LNMBACs examined, *MRP3* was up-regulated when compared to the corresponding normal lung tissue, where expression was almost undetectable.

J Pathol 2008; **216**: 75–82 DOI: 10.1002/path

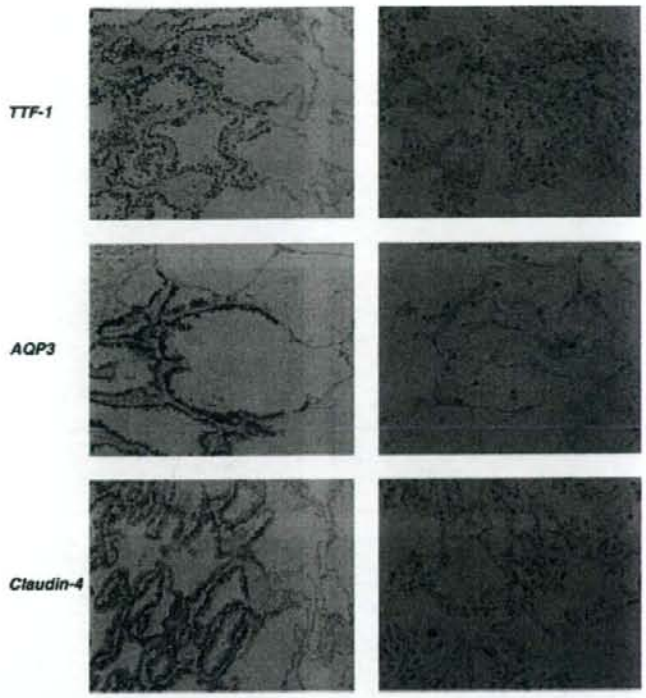

Figure 3. Immunohistochemical analysis of *TTF-1* (top), *AQP3* (middle) and *Claudin-4* (bottom) on LNMBAC (left) and normal lung (right). These genes were specifically expressed in tumour cells and could not be detected in interstitial areas in carcinoma tissue. In surrounding normal regions, histologically normal type II pneumocytes were also positive in every case, whereas type I cells were negative. The staining intensity of TTF-1 in tumour cells and normal type II pneumocytes was the same, while that of AQP3 and Claudin-4 was stronger in tumour cells

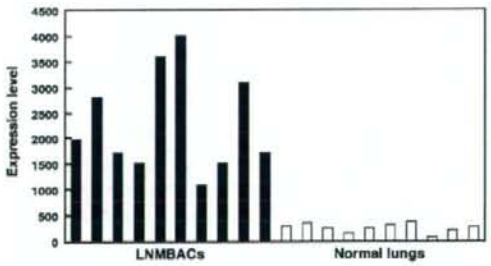

Figure 4. Expression signal of *MRP3* as measured by oligonucleotide microarray. Each bar expresses raw average difference data. All black bars representing the expression signal in LNMBACs indicate a range of about 1000–4000, whereas all white bars representing signals from normal lungs indicate undetectable expression

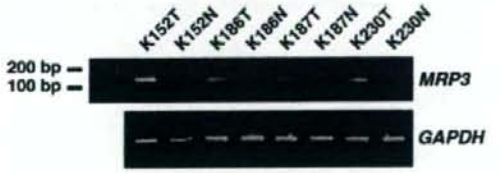

Figure 5. *MRP3* expression in LNMBAC. RT–PCR was performed to confirm the mRNA level of *MRP3* with four paired samples. The expression level of *MRP3* in LNMBAC was up-regulated when compared to that in the corresponding normal lung tissue

To determine whether *MRP3* was also expressed at the protein level, we employed a monoclonal antibody against MRP3 in an immunohistochemical study (Figure 6) and counted positively-stained cells in each lesion (Figure 7). We examined LNMBAC, the surrounding normal lung, hyperplasia and AAH. The immunohistochemical study demonstrated strong expression of MRP3 on cell membranes in LNMBACs, and most LNMBAC samples expressed MRP3 in more than 50% of tumour cells. In normal lung and hyperplasia, including type II pneumocytes, we could not detect MRP3 protein. MRP3 protein expression in AAH varied among samples; however, most samples did not express or scarcely expressed MRP3. The percentage of positive cells increased stepwise according to the progression of lung adenocarcinoma.

Discussion

In this paper we present gene expression profiling of LNMBAC and identify a distinct gene set that distinguishes tumours from normal lung tissue; these

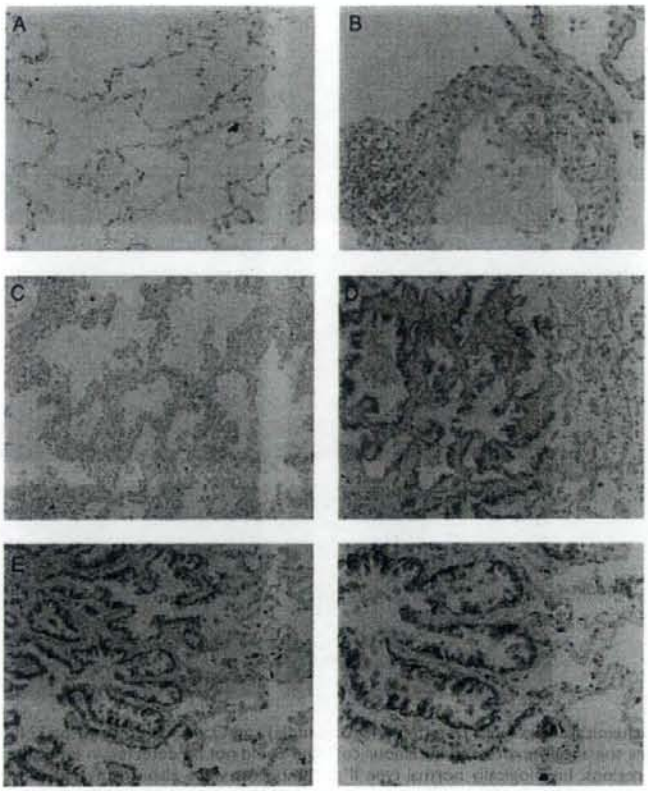

Figure 6. Immunohistochemical evaluation of *MRP3* expression in LNMBAC. Immunohistochemistry demonstrated negative expression in normal lung (A) and hyperplasia (B). Staining was also rarely detectable in AAH (C). *MRP3* expression was observed on the cell membrane in LNMBAC (D) and another case of LNMBAC (E and F). Original magnifications: ×40 (D), ×100 (E) and ×200 (F)

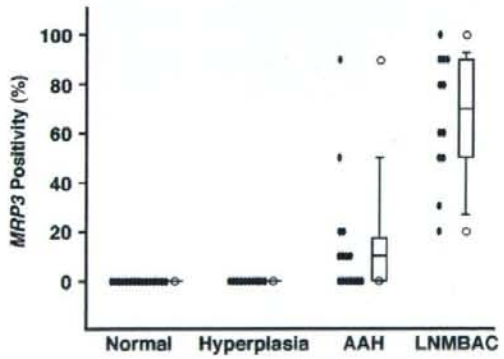

Figure 7. Relationship between immunohistochemical expression of MRP3 and LNMBAC. Scattergram and box plot show the relationship between *MRP3* immunostaining and normal lung, hyperplasia, AAH and LNMBAC. The box encompasses the 25th to 75th percentiles of results obtained, with the 50th percentile representing the median. The 5th and 95th percentiles are shown as white circles, and below and above the circles are 10th and 90th percentile whisker caps, respectively. The percentage of positive cells increased according to the stepwise progression of lung adenocarcinoma

genes particularly characterize LNMBAC. Of the up-regulated genes, we identified *MRP3* as a novel molecular marker for LNMBAC. We also identified novel type II pneumocyte lineage tumour markers.

MRP3 was identified as an up-regulated gene by two independent supervised analyses. The most remarkable feature of *MRP3* was that its expression was detected in tumour cells but not in normal type II pneumocytes. *MRP3* expression increased concomitantly with the stepwise progression from the precursor lesion of lung adenocarcinoma to AAH to LNMBAC. Moreover, *MRP3* was not detected in type II pneumocyte hyperplasia. The border between AAH and LNMBAC is unclear and sometimes varies by pathologist. This diagnostic difficulty generates severe confusion for clinical treatment; the establishment of standard management is of top priority for clinical oncologists. *MRP3* could therefore be a novel objective tumour marker for histological diagnosis and an important marker for lung cancer in the future. Our findings also suggest that *MRP3* might function as a primary factor in carcinogenesis. *MRP3* was found to be an anti-cancer drug-resistant gene in a lung cancer cell line [16]. *MRP3* belongs to the ABC transporter

J Pathol 2008; **216**: 75–82 DOI: 10.1002/path

membrane protein family, and some anti-cancer drugs induce *MRP3* expression to obtain a resistant phenotype [17–21]. However, none of the samples used in this study had received any anti-cancer drug therapy before analysis; therefore the observed *MRP3* expression was not induced by anti-cancer drugs. There is widely accepted view that BAC is less chemosensitive than other non-small cell lung carcinomas; however, this is not clearly supported by scientific evidence [22]. The hypothesis that observed *MRP3* expression in LNMBAC might produce congenital drug resistance would need further study. Recent studies have revealed that *ABCG2/BRCP*, a member of the ABC transporter family, can generate a cancer stem cell phenotype in addition to drug resistance [23,24]. If cancer stem cells also play a role in lung adenocarcinogenesis, then *MRP3* expression might be involved.

Well-established type II pneumocyte markers, such as *KL-6* (*MUC1*) and *SP-D*, are already used in clinical practice to determine the activity of interstitial pneumonia [25]. Upon expression profiling of LNMBAC, we identified several novel type II pneumocyte markers, such as *AQP3, RON* and *Claudin-4*, and it is expected that these molecules might also serve as markers for lung pathophysiology. Additionally, these markers were also expressed by tumour cells in LNMBAC; thus, they could be type II pneumocyte-lineage tumour markers. We postulate that there are two main reasons why many novel type II pneumocyte lineage tumour markers were identified by this simple comparison of expression profiles. The first reason is that LNMBACs have a relatively smaller interstitial area when compared to advanced adenocarcinomas; therefore, the expression profiles mainly represent tumour cell expression. The second reason is that LNMBACs are composed of monotonous tumour cells that pathologically resemble normal type II pneumocytes. Thus, while normal lungs are composed of a mixture of type I and type II pneumocytes and bronchiolar epithelium, the comparison of expression profiles of LMNBACs and normal lungs reflected the difference in the number of 'normal and neoplastic' type II pneumocytes. The molecular signature corresponds to the histological features; the tumour cells in LNMBACs also mimic the characteristics of type II pneumocytes at the molecular level. These findings support the hypothesis that some type II pneumocytes may be progenitor cells for adenocarcinomas of the BAC type. Immunohistological analysis also revealed that some type II pneumocyte lineage markers, such as *AQP3* and *Claudin-4*, might be over-expressed by tumour cells and may have some carcinogenic function.

In summary, we analysed the gene expression profile of LNMBAC and identified novel type II lineage tumour markers in addition to a novel tumour marker, *MRP3*, whose induction reflected the stepwise progression of lung adenocarcinogenesis. This study serves as a step toward better diagnosis and treatment of LNMBAC.

Acknowledgements

This work was supported by the Programme for the Promotion of Fundamental Studies in Health Sciences of the National Institute of Biomedical Innovation (NiBio); a Grant-in-aid from the Twenty-first Century Centre of Excellence Programme and Scientific Research on Priority Areas from the Ministry of Education, Culture, Sports, Science and Technology of Japan; a Grant-in-aid from the Third Term Comprehensive 10-Year Strategy for Cancer Control from the Ministry of Health, Labour and Welfare of Japan. We are grateful to Ken Yamazaki for his excellent technical assistance.

Supplementary material

Supplementary material may be found at the web address: http://www.interscience.wiley.com/jpages/0022-3417/suppmat/path.2383.html

References

1. Yamasaki M, Takeshima, Fujii S, Matsuura M, Tagawa K, Inai K. Correlation between morphological heterogeneity and genetic alteration within one tumor in adenocarcinomas of lung. *Pathol Int* 2000;**50:**891–896.
2. Chapman AD, Kerr KM. The association between atypical adenomatous hyperplasia and lung cancer. *Br J Cancer* 2000;**83:**632–636.
3. Kitamura H, Kameda Y, Takaaki I, Hayashi H. Atypical adenomatous hyperplasia of lung. *Am J Clin Pathol* 1999;**111:**610–622.
4. Niho S, Yokose Y, Suzuki K, Kodama T, Nishiwaki Y, Mukai K. Monoclonality of atypical adenomatous hyperplasia of lung. *Am J Pathol* 1999;**154:**249–254.
5. Nakahara R, Yokose T, Nagai K, Nishiwaki Y, Ochiai A. Atypical adenomatous hyperplasia of the lung: a clinicopathological study of 118 cases including cases with multiple atypical adenomatous hyperplasias. *Thorax* 2001;**56:**302–305.
6. Nomori H, Horio H, Naruke T, Suenuma K, Morinaga S, Noguchi M. A case of multiple atypical adenomatous hyperplasia of lung detected by computer tomography. *Japan J Clin Oncol* 2001;**31:**514–516.
7. Noguchi M, Morikawa A, Kawasaki M, Matsuno Y, Yamada M, Hirohashi S, *et al.* Small adenocarcinoma of the lung. *Cancer* 1995;**75:**2844–2852.
8. Aoyagi Y, Yokose T, Minami Y, Ochiai A, Iijima T, Morishita Y, *et al.* Accumulation of losses of heterozygosity and multistep carcinogenesis in pulmonary adenocarcinoma. *Cancer Res* 2001;**61:**7950–7954.
9. Kurasono Y, Ito T, Kameda Y, Nakamura N, Kitamura H. Expression of cyclin D1, retinoblastoma gene protein, and p16 MTS1 protein in atypical adenomatous hyperplasia and adenocarcinoma of lung. *Virchows Arch* 1998;**432:**207–215.
10. Maeshima A, Sakamoto M, Hirohashi S. Mixed mucinous-type and non-mucinous-type adenocarcinoma of the lung: immunohistochemical examination and *K-ras* gene mutation. *Virchows Arch* 2002;**440:**598–603.
11. Slebos R, Baas I, Clement M, Offerhaus J, Askin F, Hruban R, *et al.* p53 alterations in atypical alveolar hyperplasia of the human lung. *Human Pathol* 1998;**29:**801–808.
12. Bhattachrjee A, Richards WG, Staunton J, Li C, Monti S, Vasa P, *et al.* Classification of human lung carcinomas by mRNA expression profiling reveals distinct adenocarcinoma subclasses. *Proc Natl Acad Sci USA* 2001;**98:**13790–13795.
13. Garber ME, Troyanskaya OG, Schluens K, Petersen S, Thaesler Z, Pacyna-Gengelbach M, *et al.* Diversity of gene expression in adenocarcinoma of the lung. *Proc Natl Acad Sci USA* 2001;**98:**13784–13789.

14. Tomida S, Koshikawa K, Yatabe Y, Harano T, Ogura N, Mitsudomi T, *et al*. Gene expression-based, individualized outcome prediction for surgically treated lung cancer patients. *Oncogene* 2004;**23**:5360–5370.
15. Chuma M, Sakamoto M, Yamazaki K, Ohta T, Ohki M, Asaka M, *et al*. Expression profiling in multistage hepatocarcinogenesis: identification of HSP70 as a molecular marker of early hepatocellular carcinoma. *Hepatology* 2003;**37**:198–207.
16. Kool M, Liden M, Haas M, Schffer GL, Vree JM, Smith AJ, *et al*. MRP3, an organic anion transporter able to transport anti-cancer drugs. *Proc Natl Acad Sci USA* 1999;**96**:6914–6919.
17. Leonard GD, Fojo T, Bates SE. The role of ABC transporters in clinical practice. *Oncologist* 2003;**8**:411–424.
18. Fukuoka-Uesaka H, Saito Y, Maekawa K, Hasegawa R, Suzuki K, Yanagawa T, *et al*. Genetic variation of the ABC transporter gene ABCC3 in a Japanese population. *Drug Metab Pharmacokinet* 2007;**22**(2):129–135.
19. Belinsky MG, Dawson PA, Shchaveleva I, Bain LJ, Wang R, Ling V, *et al*. Analysis of the *in vivo* functions of Mrp3. *Mol Pharmacol* 2005;**68**(1):160–168.
20. Oguri T, Isobe T, Fujita K, Ishikawa N, Kohno N. Association between expression of the *MRP3* gene and exposure to platinum drugs in lung cancer. *Int J Cancer* 2001;**93**:584–589.
21. Young LC, Campling BG, Cole SPC, Deeley RG, Gerlach JH. Multidrug resistance protein MRP3, MRP1, and MRP2 in lung cancer: correlation of protein levels with drug response and messenger RNA levels. *Clin Cancer Res.* 2001;**7**:1798–1804.
22. Miller VA, Hirch FA, Johnson DH. Systemic therapy of advanced bronchiolar cell carcinoma: challenges and opportunities. *J Clin Oncol.* 2005;**23**(14):3288–3293.
23. Hadnagy A, Gaboury L, Beaulieu R, Balicki D. SP analysis may be used to identify cancer stem cell populations. *Exp Cell Res* 2006;**312**(19):3701–3710.
24. Ho MM, Ng AV, Lam S, Hung JY. Side population on human lung cancer cell lines and tumors is enriched with stem-like cancer cells. *Cancer Res* 2007;**67**(10):4827–4833.
25. Fehrenbach H. Alveolar epithelial type II cell: defender of the alveolus revisited. *Respir Res* 2001;**2**:33–46.

J Pathol 2008; **216**: 75–82 DOI: 10.1002/path

Establishment of an ovarian metastasis model and possible involvement of E-cadherin down-regulation in the metastasis

Yoshiko Kuwabara,[1,2] Taketo Yamada,[1] Ken Yamazaki,[1] Wen-Lin Du,[1] Kouji Banno,[2] Daisuke Aoki[2] and Michiie Sakamoto[1,3]

Departments of [1]Pathology and [2]Obstetrics and Gynecology, School of Medicine, Keio University, 35 Shinanomachi, Shinjuku-ku, Tokyo 160-8582, Japan

(Received February 28, 2008/Revised June 14, 2008/Accepted June 24, 2008/Online publication October 3, 2008)

Clinical observations of cases of ovarian metastasis suggest that there may be a unique mechanism underlying ovarian-specific metastasis. This study was undertaken to establish an *in vivo* model of metastasis to the ovary, and to investigate the mechanism of ovarian-specific metastasis. We examined the capacity for ovarian metastasis in eight different human carcinoma cell lines by implantation in female NOD/SCID mice transvenously and intraperitoneally. By transvenous inoculation, only RERF-LC-AI, a poorly differentiated carcinoma cell line, frequently demonstrated ovarian metastasis. By intraperitoneal inoculation, four of the eight cell lines (HGC27, MKN-45, KATO-III, and RERF-LC-AI) metastasized to the ovary. We compared E-cadherin expression among ovarian metastatic cell lines and others. All of these four ovarian metastatic cell lines and HSKTC, a Krukenberg tumor cell line, showed E-cadherin down-regulation and others did not. E-cadherin was then forcibly expressed in RERF-LC-AI, and inhibited ovarian metastasis completely. The capacity for metastasizing to the other organs was not affected by E-cadherin expression. We also performed histological investigation of clinical ovarian-metastatic tumor cases. About half of all ovarian-metastatic tumor cases showed loss or reduction of E-cadherin expression. These data suggest that E-cadherin down-regulation may be involved in ovarian-specific metastasis. (*Cancer Sci* 2008; 99: 1933–1939)

Metastasis is the major cause of death from cancer, despite significant progress in the diagnosis and clinical management of the diseases. It is urgent and essential to elucidate the mechanisms of cancer metastasis in order to improve the prognosis of cancer patients. Generally, metastasis consists of multiple events initiating invasion to the basement membrane and connective tissue, followed by migration into an adjacent blood or lymphatic vessels and the reaching of distant organs. The last step in metastasis is the arrest of circulating cancer cells and formation of tumor foci at the target organ.[1–4] Two mechanisms have been proposed underlying the multiple steps of metastasis.[5,6] One theory, that floating cancer cells in the blood or lymphatic stream are trapped in capillary vessels by mechanical constraints and grow to form secondary foci, simply correlates with the blood or lymphatic flow pattern. Metastasis of colon cancer to the liver may follow this anatomical theory, for instance; however, the other is a more complicated hypothesis based on molecular interactions between cancer cells (seeds) and the microenvironment of the target organ (soil). This 'seed and soil' theory can explain organ-specific metastasis such as the bone metastasis of prostate cancer,[7] brain metastasis of breast cancer,[8] and so on.

The incidence of metastatic ovarian tumors has been reported to comprise 7–10% of all ovarian cancer.[9,10] The common sources of ovarian metastatic tumors are the stomach, colon and rectum, appendix, breast, uterus, lung, and skin (melanoma).[11–14] Interestingly, bilateral lesions are found in 50–70% of patients,[10–12] and there are several reports of cases of intramucosal gastric cancers with ovarian metastasis.[15,16] These clinical data, which indicate the propensity of some tumor subsets for metastasis to the ovary, suggest the existence of unknown mechanisms underlying ovarian-specific metastasis.

Among metastatic tumors in the ovary, there is an interesting and controversial subset of tumors named Krukenberg tumors. The term 'Krukenberg tumor' has sometimes been loosely applied to any adenocarcinoma metastasizing to the ovary; however, most investigators used the classical criteria for the diagnosis of Krukenberg tumor as follows: (1) cancer in the ovary; (2) intracellular mucin production by neoplastic signet-ring cells; and (3) diffuse sarcomatoid proliferation of ovarian stroma.[17,18] The mechanisms that develop these morphologic alterations are not clear, but the significant stromal proliferation suggests that some tumor–stroma interactions may be involved in ovarian-specific metastasis.

To elucidate the mechanisms underlying ovarian-specific metastasis, an *in vivo* model of ovarian metastasis is definitely needed. To date, however, such a model has never been established. In our experiments, eight different human carcinoma cell lines were implanted in immune-deficient mice by transvenously and intraperitoneally. We examined the capacity for ovarian metastasis of these cell lines, and succeeded in establishing an *in vivo* ovarian-metastasis model with stromal reaction in the ovarian tumor. We further investigated whether E-cadherin down-regulation might be involved in ovarian-specific metastasis, because all cell lines revealing some capacity for metastasis to the ovary showed loss or reduction of E-cadherin expression.

Materials and Methods

Cell cultures. We used eight human carcinoma cell lines, as shown in Table 1. The characteristics and origins of MKN-28, MKN-45, MKN-74, TMK-1, and KATO-III are described elsewhere.[19,20] HGC27, HSKTC,[21] and RERF-LC-AI were purchased from RIKEN BioResource Center, Japan. HGC27 and RERF-LC-AI were maintained in MEM (Gibco/Invitrogen, Carlsbad, CA, USA) with 10% fetal bovine serum (FBS; PAA Laboratories, Ontario, Canada). HSKTC were maintained in F-12 HAM (Sigma-Aldrich, St. Louis, MO, USA) with 15% FBS and 2-mM L-glutamine. The other cell lines were maintained in RPMI-1640 (Sigma-Aldrich) with 10% FBS. All media were also supplemented with 100-μg/mL ampicillin and 100-μg/mL streptomycin. All cells were incubated at 37°C under 5% CO_2 and harvested from subconfluent cultures.

[3]To whom correspondence should be addressed.
E-mail: msakamot@sc.itc.keio.ac.jp

doi: 10.1111/j.1349-7006.2008.00946.x

Table 1. Human carcinoma cell lines inoculated into mice

Cell line	Origin
HGC27	Poorly differentiated gastric carcinoma
TMK-1	Poorly differentiated gastric carcinoma
MKN-45	Poorly differentiated gastric carcinoma
MKN-28	Moderately differentiated gastric carcinoma
MKN-74	Moderately differentiated gastric carcinoma
KATO-III	Gastric signet ring cell carcinoma
HSKTC	Krukenberg tumor
RERF-LC-AI	Poorly differentiated lung carcinoma

Animals. NOD/SCID (NOD/LtSz-scid) mice were maintained in a specific pathogen-free environment. Six- to 8-week-old mice were used in this experiment. Studies were conducted in accordance with the National Institutes of Health Guide for the Care and Use of Laboratory Animals.

Metastatic screening assays. Cells were suspended in the corresponding medium and inoculated into mice by injection into the tail vein (1×10^6 cells in 100 μL per mouse) and peritoneal cavity (1×10^7 cells in 100 μL per mouse). Mice were sacrificed when they became moribund and were evaluated for the organ distribution of established tumors. All experiments were performed under appropriate anesthesia. The resected tissues were fixed in 10% formalin, cut into 2- to 3-mm-thick slices, and embedded in paraffin for subsequent histological examination.

Immunoblotting. Cells were lysed in a buffer consisting of 25 mmol/L Tris-HCl (pH 8.0), 5 mmol/L ethylenediaminetetraacetic acid (EDTA), 125 mmol/L NaCl, 0.5% Triton X-100, 0.5% NP-40 (Sigma-Aldrich), and protease inhibitor mixture (Roche Diagnostics). After centrifugation at 20400g for 15 min, the supernatant was obtained. All 30-μg cell lysates were subjected to sodium dodecyl sulfate–polyacrylamide gel electrophoresis and then separated proteins were transferred to Hybond-P (Amersham Biosciences, Buckinghamshire, UK). After blocking, an anti-E-cadherin mouse monoclonal antibody (dilution 1:2500; Becton Dickinson, NJ, USA) or anti-β-actin mouse monoclonal antibody (dilution 1:1000; Sigma-Aldrich) was incubated for 1 h at room temperature. The membrane was incubated with a horseradish peroxidase–conjugated secondary antibody (Dako, Glostrup, Denmark) and visualized using an enhanced chemiluminescence kit (Amersham Biosciences).

Transfection. A PEF1/Myc-His vector plasmid containing the murine E-cadherin gene or an empty vector plasmid (kindly provided by Dr Shibata at the National Cancer Center Research Institute, Tokyo, Japan) was transfected into RERF-LC-AI using the Lipofectamine LTX Reagent (Invitrogen) according to the manufacturer's protocol. A neomycin resistance gene on the vectors was used to create geneticin-resistant stable clones.

Immunofluorescence. RERF-LC-AI and its transfectant clones were grown on collagen type I-coated culture slides (Becton Dickinson) and fixed in 4% formalin for 10 min. They were permealized with 0.1% Triton-X-100, blocked in 5% normal rabbit serum, and incubated with an anti-E-cadherin mouse monoclonal antibody overnight at 4°C, followed by an fluorescein-isothiocyanate–labeled secondary antibody (Dako) for 30 min at room temperature. The primary antibody was used at 1:100 and the secondary antibody at 1:50 dilution in 5% normal rabbit serum. Texas Red-X phalloidin (Molecule Probes, Eugene, OR, USA) and Hoechst (Molecule Probes) were used to visualize filamentous actin and the nucleus, respectively. Slides were examined using a Zeiss confocal laser scanning microscope (Axiovert 200 M LSM510-Software; Carl Zeiss, Göttingen, Germany).

Patients and tissue samples. To investigate clinical ovarian metastatic tumor cases, 25 operated cases and five autopsies were analyzed. In all cases, macroscopic enlargement of the ovary was observed. Sections were prepared from formalin-fixed, paraffin-embedded tissues of samples resected surgically between 1989 and 2005. This study was conducted under the approval of the Ethics Committee of Keio University, School of Medicine.

Immunohistochemistry. Each section was deparaffinized, rehydrated, and incubated with fresh 0.3% hydrogen peroxide in methanol for 30 min at room temperature. For antigen retrieval, sections were boiled in pH 6 (E-cadherin staining of mouse samples) or pH 7 (smooth muscle actin [SMA] staining and human-specific cytokeratin; CAM 5.2) citrate buffer for 10 min, or autoclaved in pH 7 citrate buffer (E-cadherin staining of human samples), or incubated in 0.1% tripsin at 37°C for 20 min (pankeratin staining). The sections were then incubated with primary antibodies for 1 h at room temperature. The primary antibodies and dilutions were as follows: anti-E-cadherin monoclonal antibody (1:5000; BD Transduction Laboratory) for mouse samples, anti-E-cadherin monoclonal antibody (1:500; HECD1[22]) for human samples, anti-AE1/AE3 monoclonal antibody (1:200; Dako), anti-SMA monoclonal antibody (1:200; Dako), and anti-CAM 5.2 monoclonal antibody (1:20; BD Transduction Laboratory). The sections were washed three times in phosphate-buffered saline, and incubated with the secondary antibody, Immpress Reagent (Vector Laboratories), for 30 min at room temperature.

Statistical analysis. The ages of the patients with clinical ovarian metastatic tumor were compared using the Mann–Whitney *U*-test. Other correlations were analyzed by the χ^2-test. All calculations were performed with ystat2000 (Igaku Tosho Shuppan, Tokyo, Japan).

Results

Examination of the capacity for ovarian metastasis in the eight cell lines and establishment of an ovarian-metastasis model. Using transvenous inoculation to NOD/SCID mice, the tumorigenicity of the eight human cancer cell lines was extremely low in our examination. Almost all cell lines did not show any tumorigenicity, including in the lung or liver. Only RERF-LC-AI, however, formed tumors in several organs (Table 2). RERF-LC-AI metastasized to the lung at 100%, which was considered to be a natural result because this cell line was originally derived from a lung cancer, and also because the lung should generally be the first organ that cells reach after injection into the tail vein. RERF-LC-AI most frequently metastasized to the ovary (67%) after the lung, and bilateral lesions were observed in one-third of ovarian metastatic cases (Table 2, Fig. 1a). Therefore, it was considered that RERF-LC-AI had a high propensity for ovarian metastasis, and that the experimental system of transvenous inoculation of this cell line to NOD/SCID mice could be used

Table 2. Organ distribution of experimental metastasis after transvenous inoculation of RERF-LC-AI

Organ							Days after inoculation
Ovary (unilateral/bilateral)	Peritoneal dissemination	Ascites	Pancreas	Liver	Lung	Bone/bone marrow	
3/5 (60%) (2/1)	1/5 (20%)	0/5 (0%)	1/5 (20%)	0/5 (0%)	5/5 (100%)	1/3 (33%)	53–94

doi: 10.1111/j.1349-7006.2008.00946.x

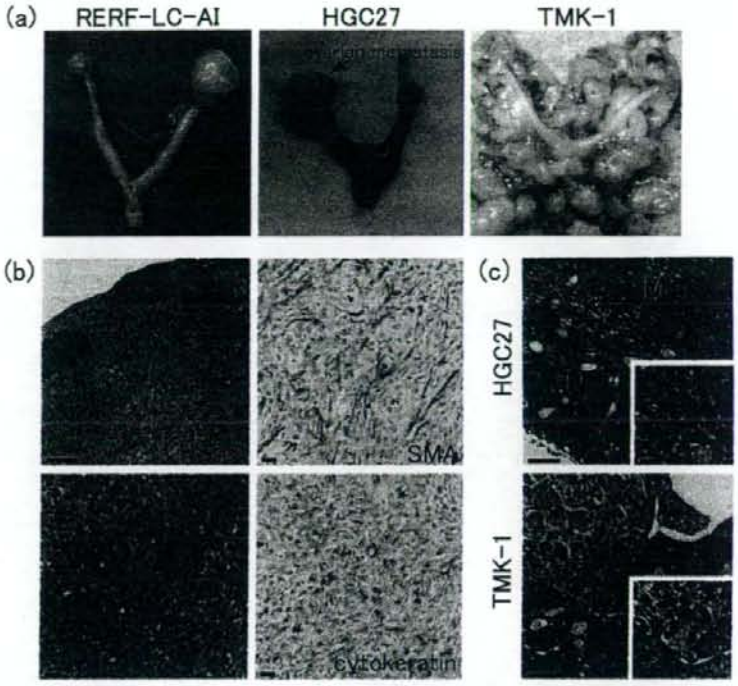

Fig. 1. Experimental metastasis by inoculation of human carcinoma cell lines. (a) Macroscopic findings of mouse ovarian tumors. Transevenous inoculation of RERF-LC-AI and intraperitoneal inoculation (i.p.) of HGC27 caused bilateral and unilateral enlargement of the ovaries, respectively. In the i.p. experiment of TMK-1, the ovaries were entirely buried in the disseminated tumor. (b) Histology and immunohistochemistry (smooth muscle actin [SMA] and human specific cytokeratin) of mouse ovarian tumors of RERF-LC-AI. Bar = 100 μm (left upper), 20 μm (the others). RERF-LC-AI cells diffusely infiltrated the ovary, and there remained only little normal ovarian tissue. In metastatic tissue, stromal reaction of ovarian fibroblasts was observed. (c) Histology of ovarian tumors established by i.p. of HGC27 and TMK-1. Insets show larger magnification of the tumor (HGC27) and the border region of tumor and normal ovarian tissue (TMK-1). HGC27 cells proliferated in the ovary (M), and normal ovarian tissue (N) remained in lower part of the figure, surrounding the metastatic tumor. This finding indicates metastasis to the ovaries, not invasion. With TMK-1, we observed the invasion of cancer cells from the surface of the ovary. Bar = 100 μm, 10 μm (insets).

Table 3. Organ distribution of experimental metastasis after intraperitoneal inoculation of the different cell lines

Cell line	Organ						Days after inoculation
	Ovary (unilateral/bilateral)		Peritoneal dissemination	Ascites	Liver	Lung	
	Metastasis	Invasion					
TMK-1	0/10 (0%)	5/10 (50%) (5/0)	10/10 (100%)	10/10 (100%)	6/10 (60%)	0/10 (0%)	21–24
HGC-27	1/9 (11%) (1/0)	0/9 (0%)	9/9 (100%)	0/9 (0%)	3/9 (33%)	3/9 (33%)	49–72
MKN-45	1/5 (20%) (0/1)	0/5 (0%)	5/5 (100%)	2/5 (40%)	1/5 (20%)	2/5 (40%)	45–86
MKN-28	0/8 (0%)	2/8 (25%) (2/0)	8/8 (100%)	6/8 (75%)	5/8 (63%)	2/8 (25%)	30–45
MKN-74	0/5 (0%)	0/5 (0%)	4/5 (80%)	0/5 (0%)	2/5 (40%)	0/5 (0%)	33–104
KATO-III	1/4 (25%) (1/0)	0/4 (0%)	2/4 (50%)	0/4 (0%)	2/4 (50%)	0/4 (0%)	101–164
HSKTC	0/12 (0%)	0/12 (0%)	1/12 (8%)	0/12 (0%)	0/12 (0%)	0/12 (0%)	119–264
RERF-LC-AI	1/4 (25%) (1/0)	0/4 (0%)	4/4 (100%)	4/4 (100%)	1/4 (25%)	1/4 (25%)	37

as an *in vivo* model of ovarian metastasis. Histologically, three-quarters of the ovarian tumors in this model demonstrated a stromal reaction, mimicking the sarcomatoid proliferation of ovarian fibroblasts in Krukenberg tumor (Fig. 1b).

Because the formation of tumor foci after transvenous inoculation of the examined cell lines was extremely rare, we also inoculated each cell line intraperitoneally. In this experiment, peritoneal dissemination was observed most often in six of the eight cell lines (Table 3). Ovarian involvement was also observed in these six cell lines; however, in the cases of TMK-1 and MKN-28, the ovaries were buried in the disseminated tumors, and the cancer cells were considered to invade the ovaries directly from predominant adjacently disseminated tumors. On the other hand, by inoculation with HGC27, MKN-45, KATO-III, and RERF-LC-AI, significant enlargement of the ovary without adjacent dissemination was observed (Fig. 1a,c). These four cell lines are considered to have some capacity for metastasizing to the ovary, but even in RERF-LC-AI, ovarian metastasis occurred at only a low percentage by intraperitoneal inoculation (i.p.). After i.p. of RERF-LC-AI, mice became moribund and were sacrificed earlier than after transvenous inoculation (37 days *vs* 53–94 days) (Tables 2 and 3). It can be speculated that in i.p. cases, peritoneal dissemination might debilitate mice so rapidly that ovarian metastasis could hardly be observed when they were sacrificed.

HSKTC, a rare cell line derived from Krukenberg tumor,[21] was also used in our examination. Unfortunately, its tumorigenicity was extremely low, even by intraperitoneal inoculation, and we could not evaluate its affinity for the ovary in *in vivo* experiments.

Down-regulation of E-cadherin in ovarian-metastatic carcinoma cell lines. To characterize the four metastatic cell lines, we searched the common features concerning gene expression. Although we examined the expression of some chemokines and their receptors, these molecules were not commonly expressed in the four cell lines. Then we focused on another molecule,

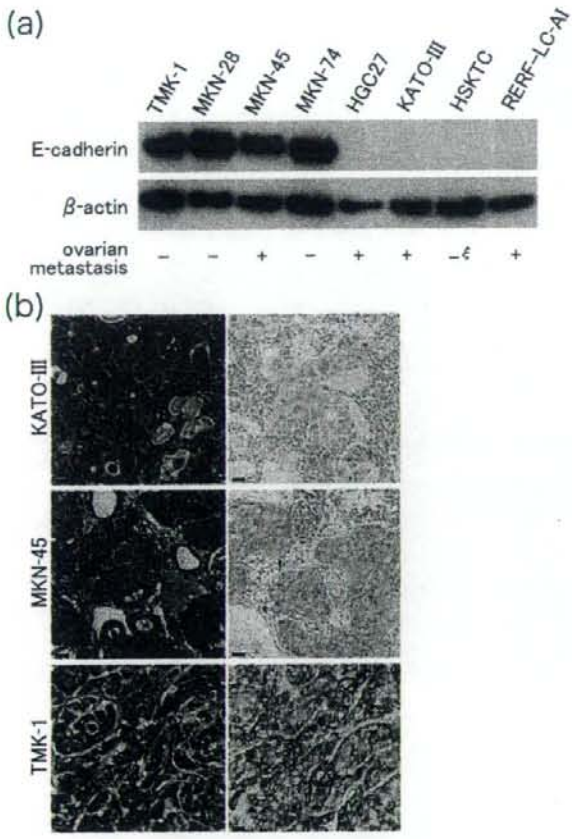

Fig. 2. E-cadherin expression in different carcinoma cell lines. (a) Immunoblot analysis of eight human carcinoma cell lines. Of the four cell lines which clearly metastasized to the ovary, all but MKN-45 demonstrated loss of E-cadherin expression. A Krukenberg tumor cell line, named HSKTC, was also negative for E-cadherin, although it showed extremely poor tumorigenicity in NOD/SCID mice (§). All non-'ovarian-metastatic' cell lines expressed E-cadherin strongly. (b) Hematoxylin–eosin staining and E-cadherin immunohistochemical staining of ovarian lesions of KATOIII and MKN-45, and disseminated tumor of TMK-1. KATO-III was negative for E-cadherin, and MKN-45 showed only weak staining of the cytoplasm. TMK-1 demonstrated positive staining of the cell membranes. Bar = 20 μm.

E-cadherin, whose down-regulation and inactivation in these cells have been reported previously.[23,24] We examined E-cadherin expression of the eight carcinoma cell lines by immunoblot analysis and immunohistochemical staining of mouse tumors. The three of four 'ovarian-metastatic' cell lines and HSKTC showed loss of E-cadherin expression in immunoblot analysis and immunohistochemistry (Fig. 2a,b). Although MKN-45, an 'ovarian-metastatic' cell line, was E-cadherin-positive in immunoblot analysis, its metastatic tumor demonstrated only weak cytoplasmic staining by E-cadherin immunohistochemistry (Fig. 2b). Dysfunctional E-cadherin by an in-frame deletion mutation of the gene in MKN-45 cells[23] seems to be involved in the cytoplasmic localization. On the other hand, non-'ovarian-metastatic' cell lines TMK-1, MKN-28, and MKN-74, were positive on E-cadherin immunoblotting and also showed strong membranous staining in immunohistochemistry.

Inhibition of ovarian metastasis by E-cadherin expression. To investigate whether E-cadherin down-regulation has any effect on ovarian metastasis, the murine E-cadherin gene was transfected into RERF-LC-AI, which showed a high propensity for metastasis to the ovary by transvenous inoculation. Transfectant clones were confirmed to express E-cadherin by immunoblot analysis (Fig. 3a), and immunocytochemistry proved the localization of E-cadherin on cell membranes (Fig. 3b). Three high-expressing clones (LC CDH1-1, -6, -8) and two empty vector-expressing clones (LC vector-3, -4) were inoculated into immune-deficient mice by intravenous injection. None of the E-cadherin transfectants showed tumorigenicity in the ovaries, while mock cells metastasized to the ovaries at high frequency (Table 4). The capacity for metastasis to other organs, such as the pancreas and lung, was maintained in all of the transfectants examined. E-cadherin expression of mouse metastatic tumors of LC CDH1-1, -6, and -8 was confirmed by immunohistochemistry (Fig. 3c). These data indicate that E-cadherin expression specifically inhibited ovarian metastasis in our model.

Classification of clinical ovarian-metastatic tumors by E-cadherin expression. In order to identify whether E-cadherin down-regulation is also observed in clinical cases, we classified 30 cases of ovarian-metastatic tumor by E-cadherin expression examined by immunohistochemistry (Table 5 and Fig. 4). Loss or reduction of E-cadherin expression was observed in 14 cases, and this subset of tumors showed significant associations with a younger population, stomach origin, bilateral involvement of the ovaries, poor differentiation, and stromal proliferation. The other 16 cases demonstrated a strong expression of E-cadherin. Most of these tumors were of colonic origin and well differentiated. Stromal proliferation was rarely observed in E-cadherin-positive cases.

Discussion

Organ-specific metastasis has been investigated intensively and the underlying mechanism has been partly elucidated in several types of carcinoma.[5] The findings of diverse molecules, such as chemokines, growth factors and so on, signal pathways, and new genes have enabled new developments in this field;[1,5] however, there has been no basic research on ovarian-specific metastasis. In the present study, we examined the capacity for metastasis to the ovary in different human carcinoma cell lines. Implantations of the cell lines into NOD/SCID mice were performed

Table 4. Organ distribution of experimental metastasis after transvenous inoculation of RERF-LC-AI transfectants

Transfectant	Organ							Days after inoculation
	Ovary (unilateral/bilateral)	Peritoneal dissemination	Ascites	Pancreas	Liver	Lung	Bone/bone marrow	
LC/CDH1-1	0/5 (0%)	1/5 (20%)	0/5 (0%)	1/5 (20%)	0/5 (0%)	5/5 (100%)	0/5 (0%)	68–163
LC/CDH1-6	0/5 (0%)	3/5 (60%)	0/5 (0%)	0/5 (0%)	0/5 (0%)	3/5 (60%)	0/5 (0%)	70–91
LC/CDH1-8	0/5 (0%)	2/5 (40%)	0/5 (0%)	5/5 (100%)	0/5 (0%)	5/5 (100%)	1/5 (20%)	53–72
LC/vector-3	4/5 (80%) (2/2)	1/5 (20%)	1/5 (20%)	3/5 (60%)	1/5 (20%)	4/5 (80%)	1/5 (20%)	31–66
LC/vector-4	3/4 (75%) (1/2)	4/4 (100%)	2/4 (50%)	3/4 (75%)	1/4 (25%)	4/4 (100%)	0/4 (0%)	66–86

doi: 10.1111/j.1349-7006.2008.00946.x